Article

Microgripper Based on Simple Compliance Configurations, Improved by Using Parameterization

Pedro Vargas-Chable [1,2], Jose Mireles Jr-Garcia [3], Sahiril Fernanda Rodriguez-Fuentes [4], Samuel Isai Valle-Morales [5] and Margarita Tecpoyotl-Torres [2,*]

1 Facultad de Ciencias Quimicas e Ingenierias (FCQeI), Universidad Autonoma del Estado de Morelos, Cuernavaca, Morelos 62209, Mexico; pedro.vargas@uaem.mx
2 Instituto de Investigacion en Ciencias Basicas y Aplicadas-Centro de Investigacion en Ingenieria y Ciencias Aplicadas (IICBA-CIICAp), Universidad Autónoma del Estado de Morelos, Cuernavaca, Morelos 62209, Mexico
3 Centro de Investigacion en Ciencia y Tecnologia Aplicada, Universidad Autonoma de Ciudad Juárez, Av. Plutarco Elias Calles #1210, Fovissste Chamizal, Ciudad Juarez, Chihuahua C.P. 32310, Mexico; jmireles@uacj.mx
4 Licenciatura en Tecnologia con areas terminales en Fisica Aplicada y Electronica, Universidad Autonoma del Estado de Morelos, Cuernavaca, Morelos 62209, Mexico; 20144009513@alumnos.uaem.mx
5 Posgrado en Ingenieria y Ciencias Aplicadas, Universidad Autonoma del Estado de Morelos, Cuernavaca, Morelos 62209, Mexico; samuel.valle@uaem.edu.mx
* Correspondence: tecpoyotl@uaem.mx

Received: 19 November 2020; Accepted: 10 December 2020; Published: 15 December 2020

Abstract: The design of a novel electrothermal microgripper device is shown, which is based on an improved chevron type actuator developed considering their elements parameterization, whose resistive model is also provided. The performance of the microgripper's parameters, such as displacement, force, and temperature distribution, with convection for the voltage range from 0 up to 5 V, is evaluated through numerical and analytical simulation. Microgripper design was also improved with aid of parameterization. The effect on the microgripper performance due to its thickness is also analyzed, finding a considerable increment in force, when thickness increases. Its main advantage is given by the simplicity of the compliance arrangement of the microgrippers jaws. Considering convection, when 5 V are applied, 37.72 °C was generated at the jaw's tips of the Improved Microgripper 2 (IMG2), implemented with silicon, this relatively low temperature increases its capabilities of application. When the IMG2 is implemented with polysilicon, its response is competitive comparing with a more complex microgripper, increase of displacement (50%) is shown, but a decrement of force (30%). The diameters allowed for the subjection objects are found between 84.64 μm and 108 μm, with weights lower than 612.2 μg. Some tests of subjection were performed using microcylinders of Au, glass ceramic, polycarbonate and carbon fiber, showing a permissible stress on them, considering its Young's modulus, as well as the total reaction force induced. All simulations were done on Ansys software. The results demonstrate the feasibility of the future microgripper fabrication.

Keywords: parameterization; compliance arrangement; displacement; temperature distribution; force; silicon; polysilicon; microparticles subjection; Ansys

1. Introduction

Microelectromechanical systems (MEMS) involve both electronic and non-electronic elements, and perform functions that can include signal acquisition, signal processing, actuation, display and

control [1]. MEMS refer to a set of microsensors and microactuators that can perceive environments and have the ability of reacting to changes in those environments, using the control microcircuits [2].

Microactuators based on different actuation principles, such as shape memory alloys, electrostatic, electrothermal, piezoelectric, pneumatic, and electromagnetic approaches, have been devised to drive MEMS microgrippers. Electrothermal actuation is widely applied in MEMS. Typically, it can generate a large output force by using low voltages [3].

The electrothermal actuation consists of the thermal expansion of the clamping arms, due to the Joule effect, in the presence of electric current. Electrothermal micro clamps have many advantages, such as wide deformation, strong clamping force, low operating voltage, and compact structure. However, the limitations of electrothermal actuators are related to the high temperature in the region close to the clamping targets, so long clamping arms must be used to dissipate the heat produced by the actuators [4], among other strategies that have been used. Microgripper performance depends on the actuation method, material properties, geometry, and kinematic behavior [5]. In this case, the work focuses on the geometry improvement, which provide an increment on jaw's displacement and in their reaction force. These parameters determine the size and weight of the subjection objects.

Compliant mechanisms can be used to design mechanisms having specific force-deflection properties, e.g., compliant constant-force mechanism, which generates a nearly constant output force in response to, say, a linear input displacement [6]. They are widely used in several areas, such as robotics and precise positioning systems. Such mechanisms can be used as motion or force amplifiers/reducers [7]. Among their well-known advantages, are no friction, light weight, no need for lubrication, and zero backlash. They can contain fewer parts or can be manufactured as one piece [8]. They are flexible structures that deliver the desired motion and force by undergoing elastic deformation as opposed to rigid-body mechanisms [9].

In microelectromechanical systems (MEMS), compliant devices offer an alternative to obtain micromechanical movements without requiring mechanical assembly. The majority of microdevices and systems rely on mechanical compliance (flexible structures) to take advantage of micromachining techniques and to meet batch production constraints [10]. They have been widely used also for microgripper design [11].

Microgrippers Actuated by Chevrons

Several examples of micro-grippers actuated by chevron actuators can be found in the literature (some of them are given in Table 1). In this work, the electrothermal microgripper will also be actuated by a chevron actuator.

More examples of microgrippers actuated by chevron are given in [11], and some patents in [12].

Silicon has been widely used for fabrication of MEMS devices, especially due to its mechanical properties, its low cost, the maturity of its knowledge, as well as its compatibility with fabrication processes of integrated circuits. Electrostatically [13–15] and mechanically [16] actuated MEMS silicon microgrippers are also reported.

From the analyzed literature, a challenge arises in relation to the improvement of the microgripper elements, not only of the chevron actuator, but also of the compliance arrangement, which is the base of each arm. This interest in due to, currently, it is possible to develop parametric analyzes reducing both the time and costs involved in the design process. The simulation software, in the parametric analysis, automatically solves complete ranges of specific variables. The graphical display of their results allows the user to detect trends, by analyzing the performance shown, and choose the most appropriate values of the variables, according to the established requirements, based on the needs of the application to which they will be destined.

Parametric design significantly reduces the time and cost of developing design processes, while guiding the development of a robust design. In complex system design processes, it is common to follow proven design methodologies, such as Model V or Smart product system design model,

where the intermediate stage, which is called Detailed Design and Optimization [17], is directly related to parametric analysis.

Table 1. State of the art of advances in micrograppers actuated by chevron actuators.

Description	Displacement (µm)	Force (µN)	Dimensions (µm)	Material	Feeding	Ref.
Electrothermal microgripper with chevron microactuator	1.39	N/A	~102 × 35 × 1	Nickel	28 mA	[18]
Microgripper with chevron microactuator	80	~200	2900 × 3500 × 45	SU-8	53 mV	[8]
Electrothermal microgripper	310.6	N/A	~13,500 × 2500 × 180	Silver/Nickel	0.26 A	[19]
Microgripper with chevron electrothermally actuated	19.2	37000	~870 × 200 × 10	Polysilicon	0–1.2 V	[20]
Electrothermal microgripper with two chevrons	40	N/A	~1300 × 530 × 4	Ni	1 V	[5]
Microgripper Based on the Cascaded V-ShapedActuators	>50	N/A	~1000 × 1500 × 20	SU-8 (with Cr/Au/Cr films)	26–28 mA	[21]
Microgripper based on chevron actuator	71.5	N/A	~3500 × 3120 × 45	Copper-SU-8-Copper	195 mV	[22]

In this paper, determinant elements of chevron actuator have been parameterized, such as its inclination angle, and the width of its shuttle, considering their effects on the displacement and the reaction force on the shuttle, for each case. In addition, the parameterization of the complete microgripper will be carried out considering the effect of the change in the values of the angles of the compliance arrangements that are decisive in the operation, as well as the length of the arms effect.

Our aim is the design of a novel and simple microgripper based on a chevron actuator, and a compliance arrangement. The content of this work is organized as follows. In Section 2, design of the elements of the microgripper are provided, as well as the conventional mathematical model of chevron actuator and the basis of the microgripper. Simulation results of the main parameters of the microgripper, a comparison with another microgripper, and some objects holding tests, are provided in Section 3. Finally, in Section 4, some concluding remarks are given.

2. Materials and Methods

Silicon is used as structural material for the microgripper design, its parameters are shown in Table 2. Polysilicon was also chosen for generalizing the obtained results and compare the performance of microgrippers, its parameters are also given in Table 2.

Table 2. Physical and mechanical properties of silicon [23–25] and polysilicon [26].

Parameters	Values for Silicon	Values for Polysilicon
Density, [kg/m^3]	2329	2320
Thermal expansion coefficient, α [1/°C]	2.568e−6	2.6e−6
Young's Modulus, E [Pa]	1.301e11	1.60e11
Poisson's ratio, υ	0.33	0.22
Bulk Modulus [Pa]	1.27e11	9.4e10
Shear Modulus [Pa]	4.89e10	6.475e10
Thermal conductivity, [W/(m/°C)]	148	34
Resistivity, ϱ [Ω*m]	1.5e−4	2.2e−5
Melting point [°C]	1414	1411.85

The schematic diagram of the proposed electrothermic chevron, which actuates the microgripper is depicted in Figure 1. Its performance will be analyzed, with the aid of an improvement process based on parametric analysis, described in the flux diagram shown in Figure 2, to take decisions about any change on the geometry. In this established process, at first, the performance parameters to improve, must be determined, as they will guide to the user's decisions. The knowledge of the possible device applications will be very useful in this determination. As second step, it is necessary to identify the determinant geometric elements on the initial device performance, because, individually, all of them will be parameterized. The graphical deployment of their results (step 3) will be useful to user, for the determination of the most suitable dimensions of the determinant elements of the geometry (step 4). Some design rules of the fabrication process, previous knowledge and expertise should be also considered in the decision making. The enhanced geometry will be determined with this selection of elements dimensions (step 5). Later, it is necessary to simulate the improved device in order to analyze its performance parameters (step 6). If the appropriated parameter values have been obtained (step 7), the process will be finished, or it will be necessary to go back to step 4 and continue again since this point, until the chosen performance parameters would have suitable values.

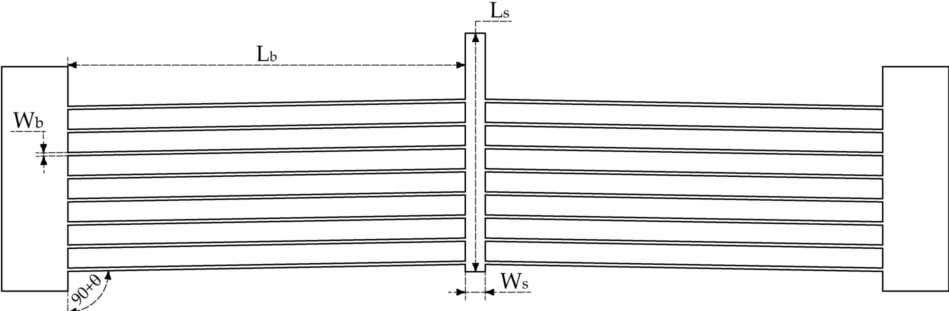

Figure 1. Chevron actuator.

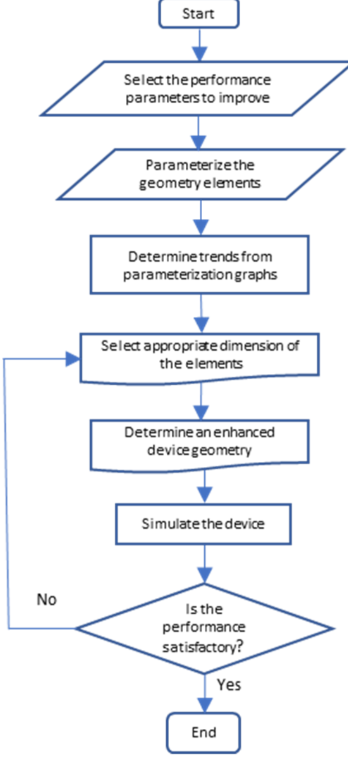

Figure 2. Flux diagram of proposed parameterization process.

As it can be observed, automated sweeps, quickly performed, generating useful information to analyze performance trends and, therefore, to select the most appropriate values of the variables under analysis, in accordance with the established requirements and conditions. Parameterization was performed without consider convection. Dimensions of the proposed chevron are given in Table 3.

Table 3. Geometrical parameters of the chevron microactuator.

Description	Variable	Dimension
Beams length (μm)	L_b	600
Beams width (μm)	W_b	5
Angle of beams (°)	θ	1°
Thickness structure (μm)	t	70
Shuttle length (μm)	L_s	660
Shuttle width (μm)	W_s	30

The properly microgripper section of the complete device was initially designed considering two structures based on simple compliance arrangements. Jaws tips were designed to favor grip, using a toothed shape. The schematic diagram of the jaws' section is shown in Figure 3, and its dimensions are given in Table 4. Thickness of the microgripper is 70 μm. Later, this microgripper would be improved, considering the determinant geometry elements on its displacement and reaction force.

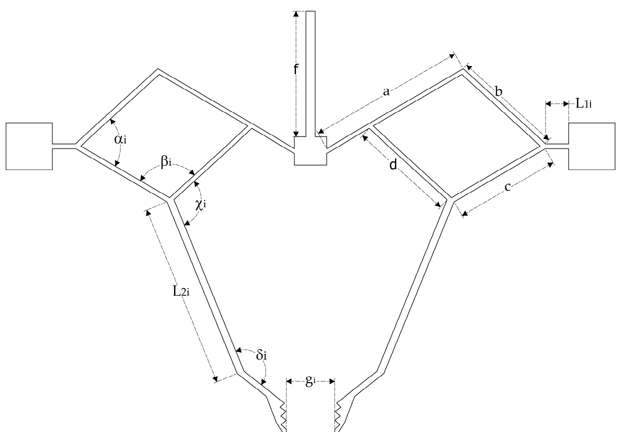

Figure 3. Schematic diagram of the initial gripper.

Table 4. Initial microgripper dimensions.

Element	Value	Element	Value
gi	86.24 μm	f	270.5 μm
a	340 μm	αi	72.5°
b	240 μm	βi	72.5°
c = d	227 μm	χi	115°
L1i	480 μm	δi	124°
L2i	50 μm		

In accordance with [11], the here proposed microgripper can be considered as part of the class 1, as it is based on lumped compliance mechanism. In this case, on a compliance rhombus frame. In [11], inside class 1, there are also shown several cases of microgrippers actuated by chevron. In [27], other example of microgripper actuated by chevron is provided, with thickness of 50 μm. Its application as part of a micropositioner is also provided. The thickness of the device here chosen (70 μm) is near to that value and is feasible to fabricate using SOI process.

Previous simulations of microgripper parameters, displacement, and force, lets us envisage the elements to be parametrized, due to immediate influence on the microgripper performance:

- The internal angles, represented by α_i and β_i, of the two symmetrical simple compliance arrangements, which are the bases of the jaws.
- The length of the arms or jaws, L_2, which initially have a length of 480 µm.
- The length of the beam, L_1, which connects the simple compliance arrangement to the anchor. Its length change has a significant impact on the displacement and force.
- The angles represented by χ_i and δ_i, also have a determinant influence on the microgripper performance.

2.1. Chevron Model

In this section, the modeling of the displacement and force for the chevron actuator is given. These variables are necessary as they support the jaw's performance.

Displacement is calculated by [28]:

$$U_y = \frac{F_y}{N\left(S^2\frac{EA}{L} + C^2\frac{12EI}{L^3}\right)} \quad (1)$$

where N is the number of beams, E is the Young's modulus, L is the beam length, F_y is the actuation force, A is the area of the cross-section, I is the inertia moment, S and C are $sin\theta$ and $cos\theta$, respectively, and θ is the aperture angle of each beam, as it is shown in Figure 1.

Inertia moment is calculated as follows [29]:

$$I = \frac{wt^3}{12} \quad (2)$$

where w is the beam's width, and t is the device thickness.

The force is obtained by [30]:

$$F_y = N\varepsilon AE \sin\theta \quad (3)$$

where all variables where previously defined, except ε, the thermal deformation, which provides the increment in the body's dimensions, due to the increment in temperature, caused by the voltage supply:

$$\varepsilon = \alpha\Delta T \quad (4)$$

where α is the thermal expansion coefficient of the corresponding material, and ΔT denotes the temperature change. Room temperature in this paper was considered as 22 °C.

Newton's second law was used to calculate the maximum mass that the micro-gripper can support. To obtain the displacement amplification factor (DAF), it is used [31,32]:

$$DAF = \frac{d_2}{d_1}, \quad (5)$$

where d_1 is the microactuator displacement and d_2 corresponds to displacement between tips.

In the literature, there are reported amplification factors in the range from 2.85 up to 50, for piezoelectric microgrippers, with applied voltages from 0 to 700 V, giving output forces from 1 µN up to 1.87 N [31,33]. For electrothermal microgripper, with nickel, amplification factor of 7.89 was reported, when two stacks of chevron actuators are used to drive two gripper arms [34].

For the electrical properties used in the microgripper design, the intensity of the electrical current I can be calculated by using Ohm's equation. The electrical resistance (R) can be determined from the well-known equation:

$$R = \rho\frac{l}{A} \quad (6)$$

where ρ is resistivity, l is the length and A is the cross-section area, respectively. The total resistance of each device is calculated in accordance with its configuration.

2.2. Resistive Modeling of the Chevron Microactuator of 8 Beams

Schematic model of chevron is given in Figure 4. Its volumetric resistive and electric models are shown in Figure 5a,b, respectively.

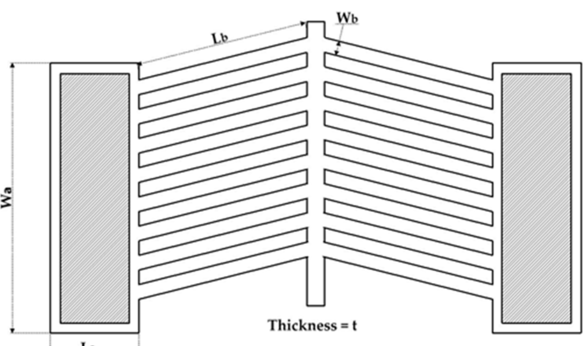

Figure 4. Schematic chevron actuator of eight pairs of beams.

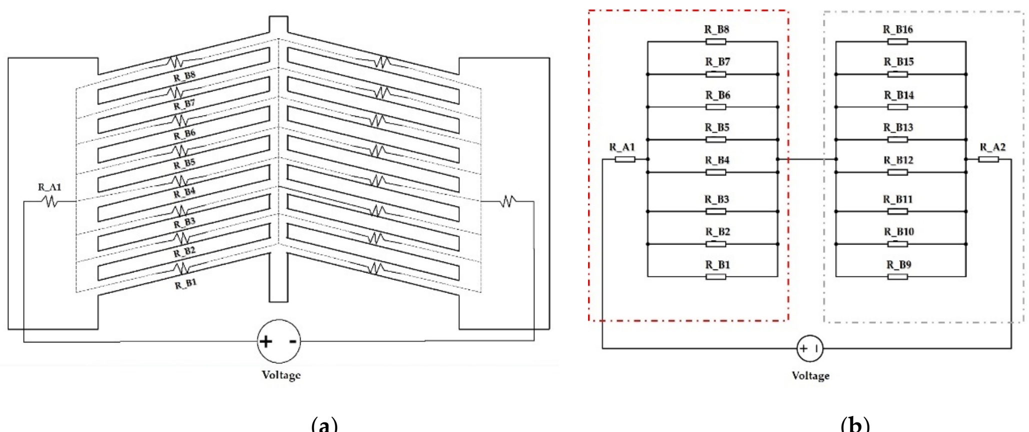

(**a**) (**b**)

Figure 5. (**a**) Resistive volumetric and (**b**) electric models of chevron actuator of eight pairs of beams.

Resistances of each beam have the same value ($R_{B1} = R_{B2} = \ldots = R_{B8} = R_B$), simplified as:

$$R_B = \rho \frac{L_b}{W_b t} \tag{7}$$

where ρ is the resistivity, L_b, and W_b are length and width of beams, and t the thickness.

The general expression that describes the total resistance (R_T) of chevron microactuator is given by:

$$R_T = N\frac{\rho}{t}\left[\frac{L_a W_b + \frac{1}{n}(L_b W_a)}{n W_a W_b}\right] \tag{8}$$

where N is the numbers of beams, W_a and L_a, are the width and length of anchor, and n is the number of the pairs of beams. It is important to mention that in the simulations, the effect on the anchor's resistance is also considered.

Other equation to calculate total resistance of a chevron with a pair of beams is given in [35]:

$$R_e = \frac{\rho_e \times 2L}{A_c} \tag{9}$$

where $L = L_{bx}/(cos\theta)$, L_{bx} is the horizontal beam component (adjusted notation), ρ_e is the electrical resistance, A_c is the cross-sectional area ($W \times t$), L, W, and t are length, width, and thickness of the beam, respectively. θ is the pre-bend angle. Equations (8) and (9) are equivalents, if in Equation (8), $N = 2$, $n = 1$, and $L_a = W_a = 1$. That means, without considering the anchor.

Calculation of stiffness constant can be obtained from [36]:

$$k = \frac{2NE(12I\cos^2\theta + AL^2\sin^2\theta)}{L^3} \tag{10}$$

2.3. Microgripper

The microgripper shown in Figure 3 is normally open, and with the chevron actuation tends to be closed. Figure 6 shows the geometry of one of its symmetrical arms. From its left side, it is observed that a small cantilever is directly joined from its guided end to a compliant rhombus frame, which is also direct joined to the extreme of the cantilever's shuttle, which provides the displacement and force to the compliant rhombus frame. This rhombus frame provides the force and displacement to jaws.

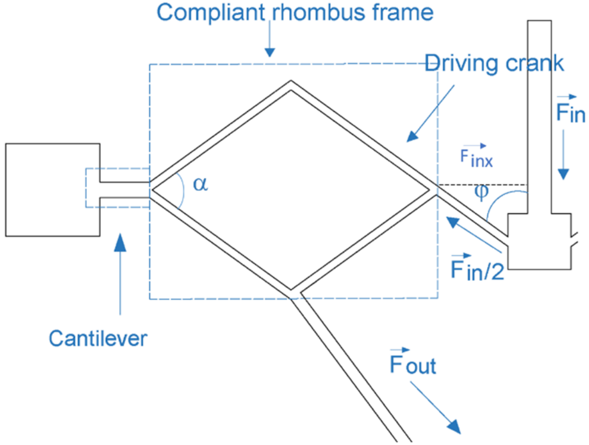

Figure 6. Elements of microgripper symmetric arm.

The longitudinal force applied to the rhombus frame, from the shuttle, is given by:

$$F_{inx} = \frac{F_{in}\sin\varphi}{2} \tag{11}$$

where φ is equal to 59.8°.

As it is known, rigidity depends on configuration, and the case of a rhombus frame is generically flexible [37,38]. This advantage was used in this design. However, it is necessary to mention that extreme cases of large deflection will not be generated, by this rhombus frame, because the magnitude of the applied force, F_{in}, is lower than 3 mN, which is not enough to tapered drastically the rhombus frame sides and change the apex angle (α) significatively, but the deflection of prismatic beams is enough to generate the jaws displacement.

3. Results

3.1. Chevron Actuator Improvement

To improve the Silicon initial microgripper, a parameterization process was first applied to chevron actuator and later, to gripper geometry. Chevron has been widely analyzed then, we only focus on its parameterization, which will be performed considering a single pair of bent beams.

It is well-known, when a potential is applied across the anchors, it causes a temperature difference due to joule heating. Variables will be called as follows: T_M is the maximum temperature, T_0,

the temperature of one anchor, V, the voltage applied across anchors, Idc, the current flow through it. The change in L, due to thermal expansion, is denoted by ΔL, and Δy is the movement of the shuttle [39]. In Figure 7, graphs obtained by parameterization of the determinant elements using Ansys, as well as the analytical calculations for chevron actuator are given. These graphs provide the trends of the actuator performance.

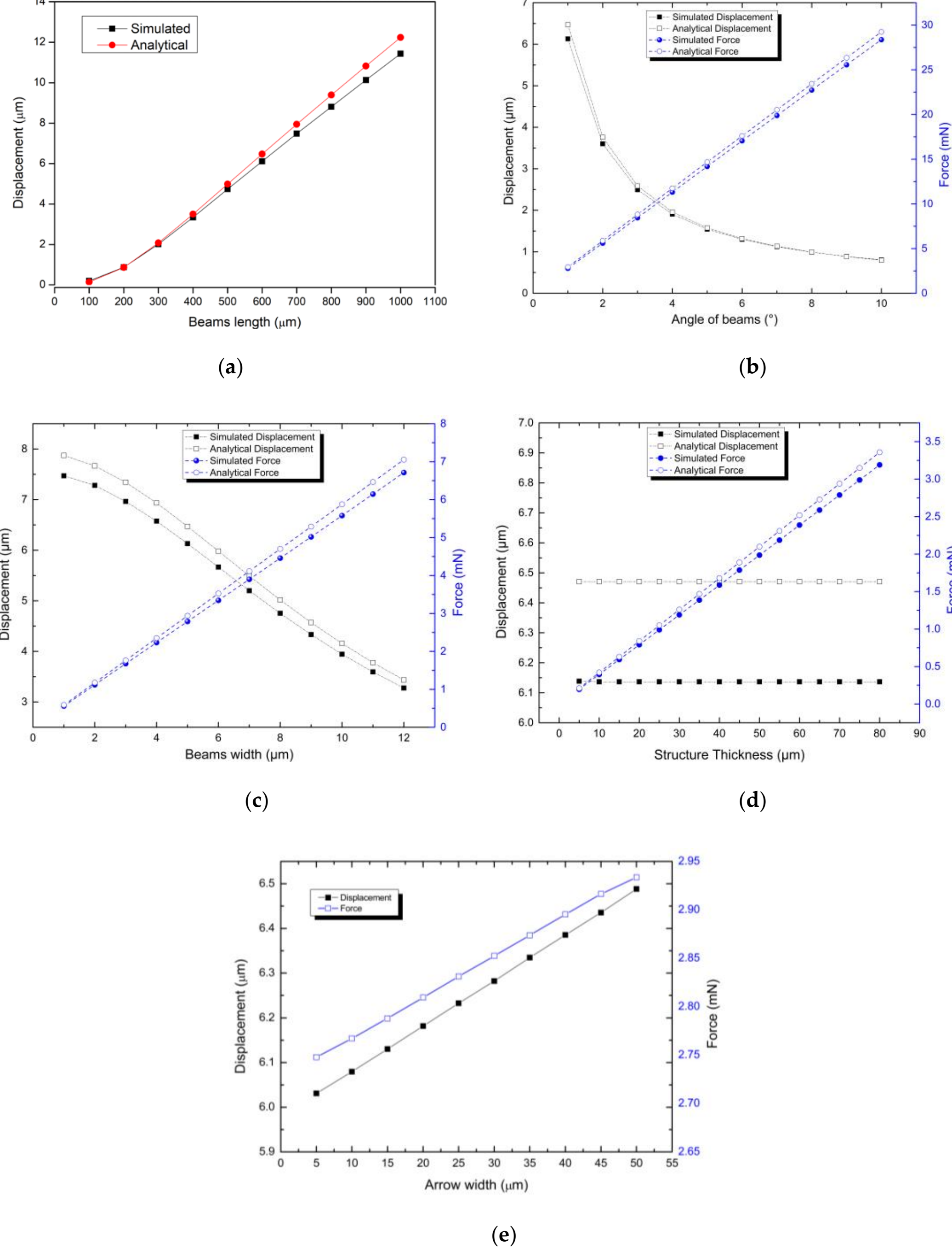

Figure 7. Chevron actuator. (**a**) Beam length vs. displacement. (**b**) Pre-bend angles of beams vs. displacement and force. (**c**) Beam width vs. displacement and force. (**d**) Structure thickness vs. displacement and force. (**e**) Arrow width vs. displacement and force.

From Figure 7a, it is observed that with beams length of 600 μm, the shuttle displacement is approximately 6 μm, which is found acceptable, considering the total length of the device, in addition,

this length is feasible for its fabrication using SOI technology. The pre-bending angle is chosen as 1°, privileging displacement over force. If we consider an angle near the intersection point of graph shown in Figure 7b, the total displacement of the microgripper is seriously decreased. From Figure 7c, it is seen that the displacement is inversely proportional to beam width, while force is directly proportional. Selection of a width beams of 5 µm was performed, again focused on displacement and maintaining an acceptable width of the structure.

Trends of displacement and force with respect to structure thickness is shown in Figure 7d, as it can be observed a linear increment of force against thickness, 70 µm is found convenient, and it compensates the selection of pre-bending angle and beam width. In addition, adequate SOI prime wafers are commercialized (Ultrasil Corp. Hayward, CA, USA), which can be used for the possible fabrication. From Figure 7e, simulated results of displacement and force against shuttle width are given, 30 µm are found suitable, as changes in force are not significant, and displacement changes are also not determinant due to the chosen scales. After this parameterization analysis, it was decided to maintain the initial values, given in Table 3, without changes.

3.2. Chevron Resistance

In Table 5, a comparison of the total resistance of chevron, is provided, with an error of 0.88%, which is an indicator of the analysis precision.

Table 5. Comparison of resistance results.

Chevron	Voltage (V)	Current Intensity (A)	Simulated Resistance, (µΩ)	Analytical Resistance, (µΩ)	Error %
8 pair of beams	2	0.03085	64.93	65.5	0.88

3.3. Initial Microgripper

The initial proposal of microgripper, shown in Figure 3, was determined by means of try and failure, without convection. ANSYS™ tool was used to improve the determinant elements of the microgripper design by using parameterization through Finite Element Analysis (FEA), without convection.

Temperature distribution generated by applying a maximum voltage of 2 V at one anchors of the chevron actuator, obtaining a maximum temperature of 112 °C, on the shuttle. One anchor is considered at room temperature (22 °C). At this maximum temperature, ΔT_M = 112 °C − 22 °C = 90 °C is obtained.

The displacement obtained applying a maximum voltage of 2 V is 9.02 µm in each jaw. The thickness of the structure corresponds to 70 µm, and the reaction force obtained is 3795 µN. When the simulation is performed considering a thickness of 15 µm, the reaction force is 795 µN. As can be seen, for a thickness of 70 µm, the increase in force is considerable (477.36%).

3.4. Performance of Initial Microgripper

In the performance analysis of the initial and improved microgrippers, three conditions were considered:

1. Anchors are fixed
2. Room temperature was applied to one of the anchors (300 °K)
3. Convective heat flux was also considered (20,000 W/m^2 °K)

Under thermal convection, the heat is transferred by a moving fluid, and is usually the dominant form of heat transfer in liquids and gases. Condition number 3, which was considered as a rule of thumb, establishes that for dimensions less than 1 mm, there will likely not be any free convective currents [40]. If the surrounding fluid is a liquid, the range of the forced heat transfer coefficients are much wider. For free convection in a liquid $h \approx 50$ to 1000 W/m^2 °K is the typical range. Constant h is

the film coefficient of heat transfer coefficient. For forced convection, the range is even wider $h \approx 50$ to 20,000 W/m^2 °K. In this case, air was considered as the fluid.

In Ansys, the procedure to perform convection analysis, is described as follows: in steady-state thermal-electric conduction, convection is inserted, frontal device's face is chosen, later *h*, the value of fluid considered in forced convection, is added, and finally the ambient temperature is stablished.

Temperature distribution of initial microgripper against applied voltage is given in Figure 8, under convection. From Figure 8, is possible to observe the variation of the maximum temperature, with the applied voltage. A voltage sweep from 0 to 10 V was performed, which generates a maximum temperature of approximately 497 °C, on the shuttle. The applied voltage parameterization was carried out, in this case, to analyze its effect on the temperature on shuttle and jaws (Figure 8a,b), as well as on the displacement generated in the jaws of the clamp and their reaction force (Figure 9). Due to this response, it was selected to apply only 5 V. Temperature distribution in the microgripper, obtained with this voltage, is shown in Figure 8c.

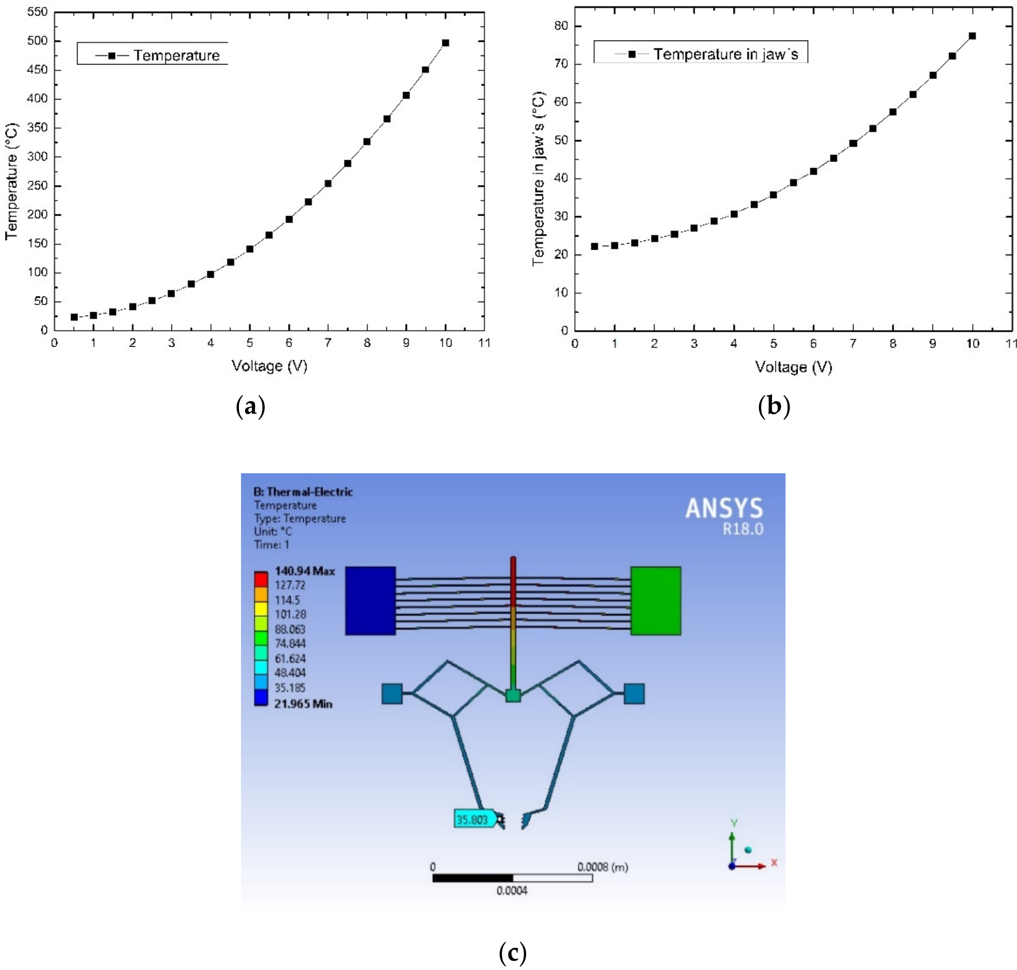

Figure 8. Temperature at (**a**) shuttle and (**b**) jaw's microgripper vs. applied voltage. (**c**) Temperature distribution of initial microgripper @ 5 V.

In Figure 9, a voltage sweep from 0 to 10 V is also applied. A non-linear increase in displacement is observed. The maximum displacement at 5 V, is 12.2 µm, considering both jaws, so the maximum diameter of the clamping objects can be of 24.4 µm. Some examples of microtubes in this range can be found at [41]. In the same Figure, the graph of voltage vs. force is displayed, with similar tendency. About the relationship between thickness versus reaction force, from Figure 10, a quasilinear dependence is observed. General data are given in Table 6.

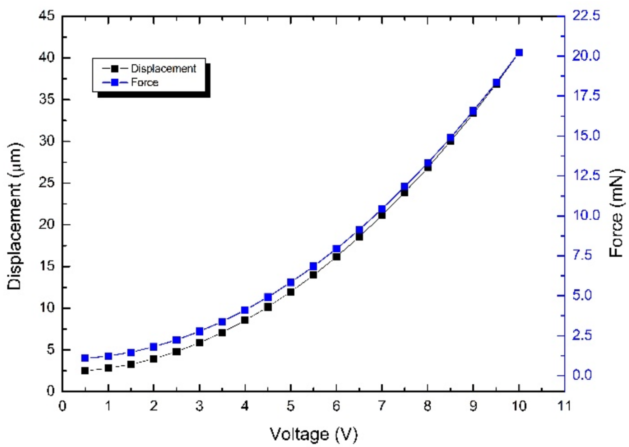

Figure 9. Voltage vs. displacement and force at a jaw of initial microgripper.

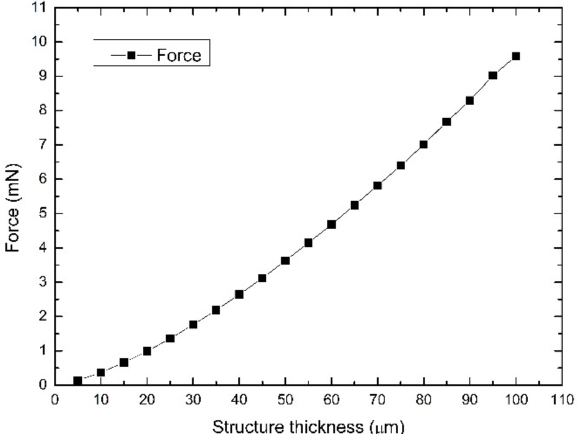

Figure 10. Structure thickness vs. reaction force.

Table 6. Values of determinant elements and parameters of the silicon initial and improved microgrippers @ 5 V, with convection.

Elements and Performance Parameters	Initial Microgripper	IMG1 (Focus on Displacement)	IMG2 (Focus on Force and Aperture)
α, [°]	72	72	72
β, [°]	107	107	107
χ, [°]	115	110	110
δ, [°]	129	150	150
L1, (μm)	50	50	50
L2, (μm)	480	350	400
Directional displacement *, (μm)	X: 19, Y: 13.6, Z: 7.6×10^{-3}	X: 21, Y: 14.6, Z: 2.6×10^{-3}	X: 19.4, Y: 13.4, Z: 7.8×10^{-3}
Total displacement *, (μm)	24.4	26	23.32
Directional reaction force, [mN]	X: 10.38×10^{-3}, Y: 5.8, Z: 0.11×10^{-3}	X: 18×10^{-3}, Y: 6.4, Z: 1.9×10^{-3}	X: 21.3×10^{-3}, Y: 6.59, Z: 3.05×10^{-3}
Total reaction force [mN]	5.8	6.49	6.6
Initial opening (g_i) (μm)	86.24	78	108
Final opening (μm)	61.84	52	84.64
Displacement amplification factor (DAF)	2.9	3.1	2.84

NOTE: *: It considers both jaws.

3.5. Parameterization of the Initial Microgripper Elements without Convection

Graphs of parametrization results of angles α, β, χ, and δ, and lengths L_1 and L_2, versus displacement and force, are given in Figure 11. They are useful to determine improved geometries of the initial microgripper.

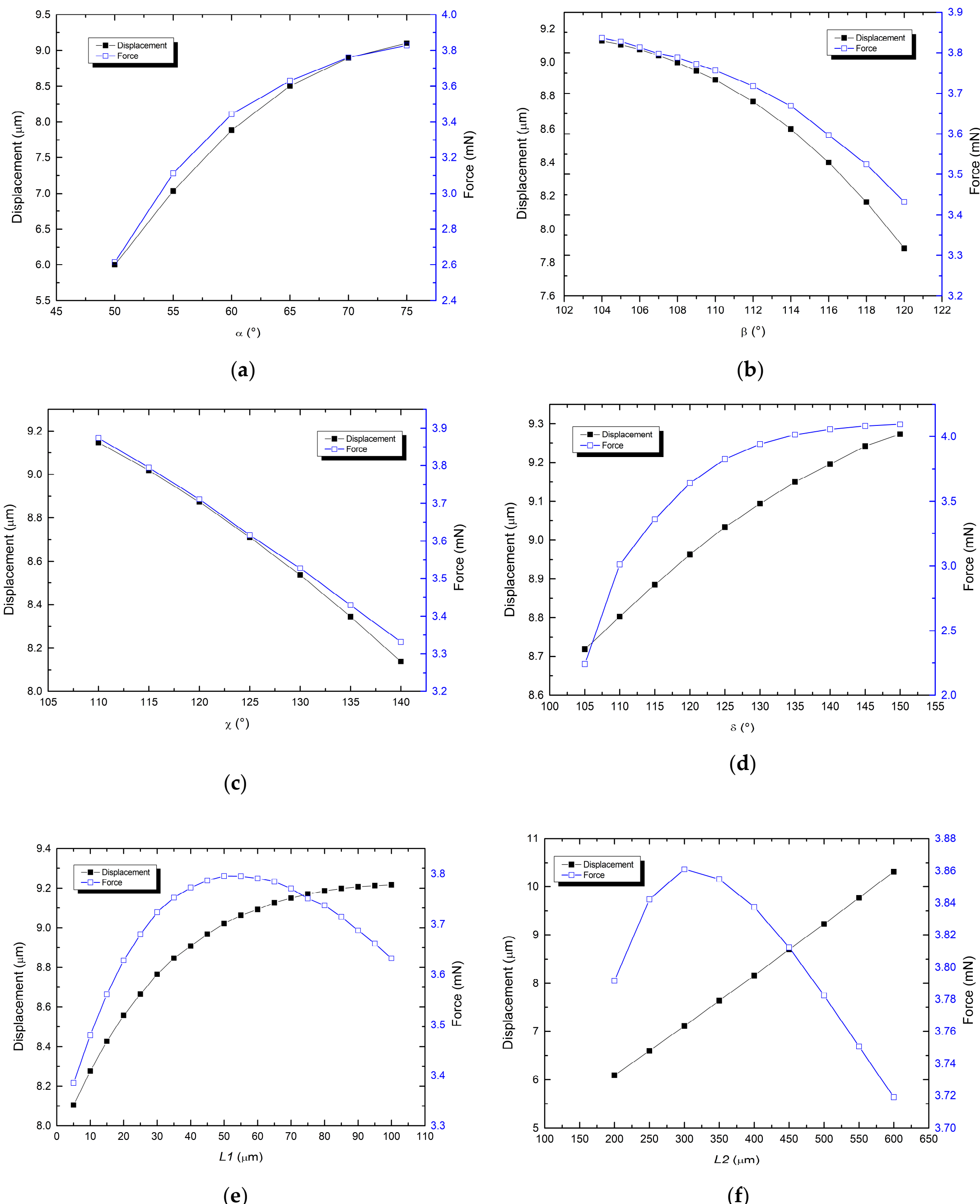

Figure 11. Microgripper. (**a**) α angle, (**b**) β angle, (**c**) χ angle, and (**d**) δ angle vs. displacement and force, respectively. (**e**) L_1 and (**f**) L_2 vs. displacement and force, respectively.

About the angle's selection, from Figure 11a,b that the initial value of the angles α and β, are very close to the maximum values indicated in the corresponding graphs, so it was decided to conserve them. In the case of χ, shown in Figure 11c, although the change in displacement is not so great, it is slightly significant in the case of force, so it was considered to take a value of 110°.

For the δ angle, the behavior of displacement is like the previous case, but it is significant for the case of force, which determines the new value of this angle (150°). About the L_1 length (Figure 11e), it is observed that it is at the right point to obtain the greatest displacement, although the force is slightly less than that the achieved at 100 µm. Then, its initial value was not changed.

For L_2 (Figure 11f), the initial value is close to the maximum displacement, without greatly sacrificing force (Improved Microgripper 1, IMG1). If the length value that allows maximum displacement is selected, the initial opening of the gripper would be very closed, which depends on the purpose for which it is intended.

If it is desired to maintain an opening like the initial one, the length of L_1 value corresponding to Improved Microgripper 2 (IMG2) can be chosen, where, in addition, provides an improvement in strength, which may be desirable for another application. Dimensions of improved microgrippers 1 and 2, as well as their parameters are shown in Table 6.

3.6. Performance of Improved Microgripper 2, (IMG2)

Dimensions for IMG2 are given in Table 7. Its displacement response and reaction force when a voltage sweep from 0 to 10 V is applied are given in Figure 12. Its temperature distribution at 5 V is given in Figure 13. General data of the IMG2 performance are also given in Table 7.

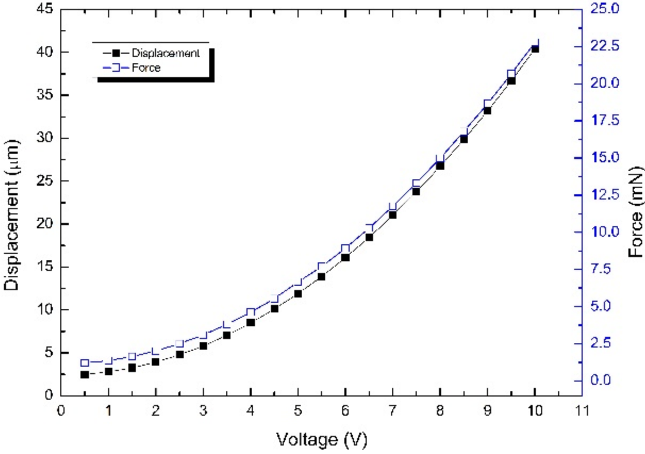

Figure 12. Displacement and force for IMG2.

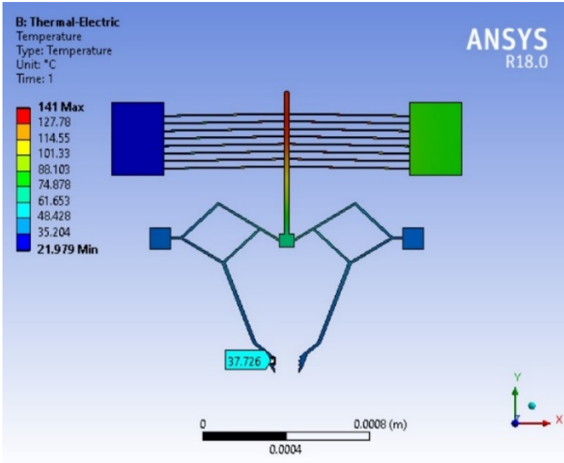

Figure 13. Temperature distribution of IMG2.

Table 7. Dimensions of the improved microgripper 2 (IMG2).

Element	Value	Element	Value
g	108 µm	f	270.5 µm
a	340 µm	α	72 °
b	240 µm	β	107°
c = d	227 µm	χ	110°
L_1	50 µm	δ	150°
L_2	400 µm		

From Table 6, it is observed that both improved grippers exceed the initial gripper force and displacement parameters. The total displacement between the jaws is greater for IMG1, while the force in IMG1 and IMG2 is greater than initial microgripper. The initial and final opening between the jaws is greater in the case of IMG2.

In all cases, from directional displacement on Z axis, it is observed that the out-of-plane deflection is minimal, providing a minimal cross axis sensitivity in this direction [42], which could represent a great advantage, because this characteristic would avoid the realignment during the operation. For the case of IMG2, the cross-axis sensitivity in this axis is 0.04%.

3.7. Comparison of Microgrippers

When IMG1 and IMG2 are implemented in polysilicon, their DAF, are 2.6 and 3.26, respectively, applying 2 V. A comparison of IMG2 with other microgrippers were performed (top part of Table 8). With Polysilicon, IMG2, comparing with the one shown in [20], allows to observe that at 50% of applied voltage, IMG2 shown larger value of displacement (75%), but lower force (30%). Temperature on chevron is similar, but in jaws, temperature is lower (15%). It is important to mention that [5] is actuated by two chevrons, and implemented in metal, for this reason, it shows, in general, a better performance at lower applied voltage. An additional advantage of the proposed gripper is its simplicity.

Table 8. Comparison with other electrothermal microgrippers.

Ref.	No. of Chevron Actuators (Beam length (L), width (W), (µm))	Total Dimensions (µm)	Material	Total Displacement (µm)	Force, mN	Temp. on Jaws (°C)	Applied Voltage (V)
			Without convection				
[43]	2 chevrons (L = 265, W = 10)	1015 × 520 × 10	Al	32.4	N/A	402	0.2
[5]	2 chevrons (L = 150 and W = 5, L = 50 and w = 4)	1100 × 400 × 10	Ni	~40	N/A	~698 on the device	1
[20]	2 chevrons (L= 400, W = 10)	870 × 10	PolySi	19.2 @ 1V	17	~248.85	1.2
IMG2	One chevron (L = 600 W = 5)	846.1 × 1314.1 × 70	PolySi	33.64	13	213.76	0.6
			IMG1 and IMG2, with convection				
IMG1	One chevron (L = 600 W = 5)	846.1 × 1314.1 × 70	Si	26	6.49	35.29	5
IMG2	One chevron (L = 600 W = 5)	846.1 × 1314.1 × 70	Si	23.32	6.6	37.26	5
IMG1	One chevron (L = 600 W = 5)	846.1 × 1314.1 × 70	PolySi	33.38	13.6	23.86	2
IMG2	One chevron (L = 600 W = 5)	846.1 × 1314.1 × 70	PolySi	40.66	17.8	25.21	2

The bottom part of Table 8 provides a comparison of IMG1 and IMG2, implemented in silicon and polysilicon. With the last material, the grippers provide bigger values on displacement and force,

than in the case of silicon, at lower voltage. With polysilicon, improved MG2 shows larger parameters than improved MG1, simulated with the same material.

On the other hand, technical details about FEA analysis are provided in Table 9.

Table 9. Technical details about FEA.

<table>
<tr><th rowspan="2">Device</th><th rowspan="2">Solver Target</th><th rowspan="2">Element Type/ Mesh</th><th rowspan="2">Face Sizing with Element Size</th><th colspan="3">Inflation</th><th colspan="2">Convergence</th><th rowspan="2">Total Mass [kg]</th></tr>
<tr><th>Transition Ratio</th><th>Max. Layers</th><th>Growth Rate</th><th>No. of Total Nodes</th><th>No. of Total Elements</th></tr>
<tr><td>Silicon initial micro-gripper</td><td rowspan="5">Mechanical APDL</td><td rowspan="5">SOLID 187/Refinement Controlled program (Tet10)</td><td rowspan="5">1.5e−6</td><td rowspan="5">0.272</td><td rowspan="5">5</td><td rowspan="5">1.2</td><td>984,826</td><td>133,633</td><td>0.482e−7</td></tr>
<tr><td>Silicon IMG1</td><td>100,6675</td><td>136,535</td><td>0.4852e−7</td></tr>
<tr><td>Silicon IMG2</td><td>35,771</td><td>16,428</td><td>0.474e−7</td></tr>
<tr><td>Polysilicon IMG1</td><td>157,4935</td><td>321,710</td><td>0.462e−7</td></tr>
<tr><td>Polysilicon IMG2</td><td>100,1318</td><td>135,999</td><td>0.455e−7</td></tr>
</table>

3.8. *Frequency Response of IMG2, Implemented in Silicon*

Modal analysis is performed to know the 3D microgripper mode shapes and its natural frequencies (Table 10, Figure 14). This knowledge allows us to avoid the vibration of the microgripper at any of its natural frequencies.

Table 10. Natural frequencies of modal forms.

Modal Form	Natural Frequency (Hz)	Modal Form	Natural Frequency (Hz)
1	3.1633e4	4	6.8518e4
2	4.2130e4	5	7.0186e4
3	6.6395e4	6	1.2667e5

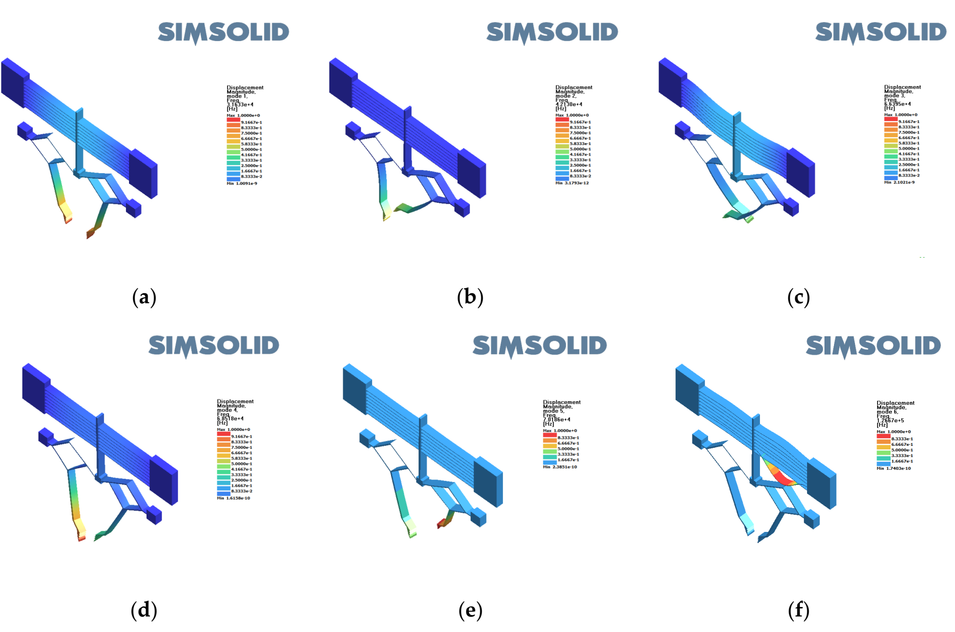

Figure 14. The first to sixth modal forms of IMG2 (**a**–**f**).

From modal forms given in Figure 14 and Table 10, it is recommended that the microgripper operates at frequencies lower to 31.633 Hz, corresponding to first modal frequency, which coincides with

the expected performance of the microgripper. Regarding the analysis confidence, in [44], after analysis of other two methods, the authors concluded that their results confirmed Finite Elements Analysis as the most recommended method and used it to study complex structures.

3.9. Holding Microparticles with Silicon and Polysilicon IMG2

Figure 15 shows results of simulation, by FEA, of the IMG2 implemented with silicon, showing it holding a microparticle. Simulation was also made with polysilicon. Results of both cases are given in Table 11, which shows the generated stress and the reaction force into microparticles of Au, glass ceramic, polycarbonate and carbon fiber (with Young's modulus, in GPa, of 78.5, 91, 0.238, and 230, respectively). In general, microparticles produces slightly lower values of stress, and total reaction forces into microparticles for the case of silicon IMG2. The lowest values of stress and reaction force correspond to the polycarbonate particle, and the largest values of both parameters correspond to carbon fiber particles. From these results, all particles under holding could be manipulated without damaging them.

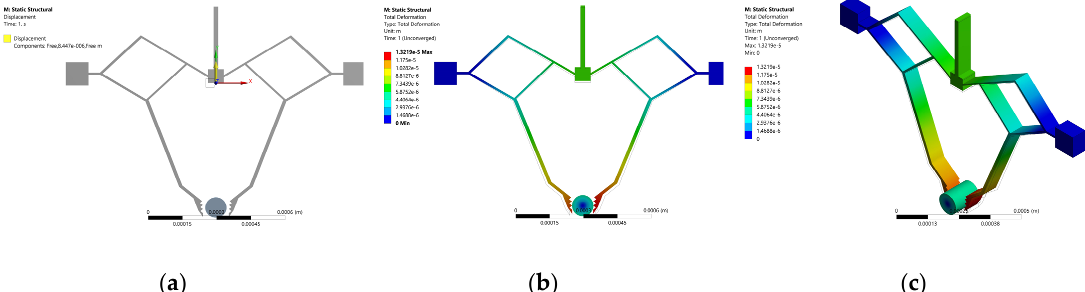

(**a**) (**b**) (**c**)

Figure 15. (**a**) Front view of the device with the microparticle positioned between the jaws. Results by FEA, of the PolySi MG2 (**b**) holding the microparticle, and (**c**) isometric view.

Table 11. Results by finite element of the IMG2, implemented with silicon and polysilicon, holding a microparticle made with different materials.

	Silicon IMG2			
Parameters	**Gold**	**Glass Ceramic**	**Polycarbonate**	**Carbon Fiber**
Stress [MPa]	2.8271	2.0314	1.3611	6.35
Total Reaction Force into microparticles [mN]	18.10	47.58	2.3264	67.81
	Polysilicon IMG2			
Stress [MPa]	3.4202	2.4695	1.3452	7.7421
Total Reaction Force into microparticles [mN]	18.237	47.175	2.3917	80.804

Simulation conditions for the manipulation of the microparticles shown in Figure 15, performed with Ansys Workbench, are given in Table 12, providing a description of the complete performed process.

Table 12. Simulation conditions for the manipulation of the microparticles, using Ansys Workbench.

<table>
<tr><td colspan="7">Toolbox → Static Structural → Project → Model → Assign materials to items → connections</td></tr>
<tr><th colspan="2">Connections</th><th colspan="2">Scope</th><th colspan="2">Definition</th><th>Advanced</th></tr>
<tr><td colspan="2">Contacts</td><td colspan="2">Contact = 1 body->
microparticle selection
Target = 16 faces of gripper</td><td colspan="2">Type = Rough
Behavior = Asymmetric</td><td>Pinball region = Radius
Pinball radius = 9e–5</td></tr>
<tr><td colspan="7">Toolbox → Static Structural→ Project →Model → Assign materials to items → connections → Mesh</td></tr>
<tr><th>Physical preferences</th><th>Sizing</th><th>Quality</th><th>Smoothing</th><th>Nodes</th><th>Elements</th><th>Advanced</th></tr>
<tr><td>Mechanical</td><td>Default</td><td>Target quality =
Default (0.05)</td><td>Medium</td><td>15534</td><td>7031</td><td>Pinball region = Radius
Pinball radius = 9e–5</td></tr>
<tr><td colspan="7">Toolbox → Static Structural→ Project →Model → Assign materials to items → connections → Mesh→ Static Structural</td></tr>
<tr><th colspan="2">Fixed support</th><th colspan="2">Displacement</th><th colspan="2">Frictionless support</th><th>Elastic support</th></tr>
<tr><td colspan="2">Geometry = 10 faces only
pads</td><td colspan="2">Component
X = free,
Y = 8.447 µm (in shuttle),
Z = free</td><td colspan="2">Scope geometry = 1 face
cylindrical</td><td>Scope geometry = 3 faces,
Foundation stiffness =
Specific for each
microparticle material</td></tr>
</table>

4. Conclusions

An important feature of the proposed microgripper is its configuration based on the arrangement of two simple compliant rhombus frame used at the base of each of the jaws. To improve its response, parameterization process was performed for chevron actuator and the microgripper, in both cases, without convection. With a thickness of 70 µm, the reaction force of the microgripper is compensated, considering the other design elements selection, which was focused on displacement.

Parameterization processes are very useful to improve geometries. It provides graphical information, which aid the user's decision making. It is also necessary, to corroborate the complete device performance in order to have a final decision.

To analyze the main performance parameters of the microgripper, convection was considered. Based on the initial microgripper, two improved microgrippers were developed (IMG1 and IMG2), simulated with silicon and polysilicon. In the last case, microgrippers have bigger values of displacement and force, even though they are feed with lower voltage. The comparison of IMG2 with a more complex microgripper found in literature, shows a larger value of displacement (50%), but a lower value of force (30%).

From the jaw's displacement and reaction force, the diameters allowed for the subjection objects are found between 84.64 µm and 108 µm, using IMG2, with weights lower than 612.2 µg. Some tests of microparticles holding were performed with IMG2, using as subjection objects to microcylinders of Au, glass ceramic, polycarbonate and carbon fiber, showing the stress on them, as well as the total reaction force induced, with permissible values in accordance to their mechanical properties, avoiding generating a damage on them.

It is important to note that the temperature in the jaws of IMG2, implemented with Polysilicon, applying 0.6 V to chevron actuator, is of 231.76 °C, but when convection and a feed of 2 V, are considered, a temperature in jaws is reduced to 25.21 °C. In both cases, these temperatures are not extreme, and are suitable for several kind of objects.

As future work, it is considered the fabrication of IMG2 using silicon or polysilicon. It is also possible to improve the microgrippers performance using other materials or reinforce the design, implementing additional structural elements.

Author Contributions: M.T.-T.: Conceptualization of research and microgripper design, formal analysis, methodology, writing, and supervision. J.M.J.-G.: Resources, methodology, and formal analysis. S.F.R.-F. and S.I.V.-M.: Research, writing, review, and editing. and P.V.-C.: formal analysis, simulation, validation,

and collaboration on microgripper design. All authors have read and agreed to the published version of the manuscript.

Funding: This research was funded by Consejo Nacional de Ciencia y Tecnologia, CONACyT, grant reference number A1-S-33433. "Proyecto Apoyado por el Fondo Sectorial de Investigación para la Educación".

Acknowledgments: Authors acknowledge to Andrés Ferrara-Bello for his recommendations. S. I. Valle-Morales is grateful for the support of CONACyT, for his studies scholarship, under grant 1045277.

Conflicts of Interest: The authors declare no conflict of interest.

References

1. Stephen, D.S. *Microsystem Design*; Springer: Boston, MA, USA, 2001; p. 4.
2. Varadan, V.K.; Varadan, V.V. Microsensors, microelectromechanical systems (MEMS), and electronics for smart structures and systems. *Smart Mater. Struct.* **2000**, *9*, 953–972. [CrossRef]
3. Jia, Y.; Xu, Q. MEMS Microgripper Actuators and Sensors: The State-of-the-Art Survey. *Recent Pat. Mech. Eng.* **2013**, *6*, 132–142. [CrossRef]
4. Iamoni, S.; Somà, A. Design of an electro-thermally actuated cell microgripper. *Microsyst. Technol.* **2014**, *20*, 869–877. [CrossRef]
5. Luo, J.K.; Flewitt, A.J.; Spearing, S.H.; Fleck, N.A.; Milne, W.I. Comparsion of microtweezers based on three lateral thermal actuator configurations. *J. Micromech. Microeng.* **2005**, *15*, 1294–1302. [CrossRef]
6. Bernardoni, P.; Bidaud, P.; Bidard, C.; Gosselin, F. A new compliant mechanism design methodology based on flexible building blocks. In Proceedings of the SPIE Smart Structures and Materials + Nondestructive Evaluation and Health Monitoring, San Diego, CA, USA, 14–18 March 2004; pp. 244–254.
7. Hricko, J.; Havlík, Š. Compliant Mechanisms for Motion/Force Amplifiers for Robotics. In *Advances in Intelligent Systems and Computing*; Springer Science and Business Media LLC: Cham, Switzerland, 2020; pp. 26–33.
8. Chu, J.; Zhang, R.; Chen, Z. A novel SU-8 electrothermal microgripper based on the type synthesis of the kinematic chain method and the stiffness matrix method. *J. Micromech. Microeng.* **2011**, *21*, 054030. [CrossRef]
9. Howell, L.L. *Compliant Mechanisms*; John Wiley and Sons, Inc.: New York, NY, USA, 2001.
10. Kota, S.; Hetrick, J.; Li, Z.; Saggere, L. Tailoring unconventional actuators using compliant transmissions: Design methods and applications. *IEEE/ASME Trans. Mechatron.* **1999**, *4*, 396–408. [CrossRef]
11. Verotti, M.; Dochshanov, A.; Belfiore, N.P. A Comprehensive Survey on Microgrippers Design: Mechanical Structure. *J. Mech. Des.* **2017**, *139*, 060801. [CrossRef]
12. Mekid, S.; Bashmal, S.; M Ouakad, H. Nanoscale manipulators: Review of conceptual designs through recent patents. *Recent Patents Nanotechnol.* **2016**, *10*, 44–58. [CrossRef]
13. Chen, B.K.; Zhang, Y.; Sun, Y. Active Release of Microobjects Using a MEMS Microgripper to Overcome Adhesion Forces. *J. Microelectromech. Syst.* **2009**, *18*, 652–659. [CrossRef]
14. Chen, L.; Liu, B.; Chen, T.; Shao, B. Design of hybrid-type MEMS microgripper. In Proceedings of the 2009 International Conference on Mechatronics and Automation, Changchun, China, 9–12 August 2009; pp. 2882–2887.
15. Yamahata, C.; Collard, D.; Legrand, B.; Takekawa, T.; Kumemura, M.; Hashiguchi, G.; Fujita, H. Silicon Nanotweezers with Subnanometer Resolution for the Micromanipulation of Biomolecules. *J. Microelectromech. Syst.* **2008**, *17*, 623–631. [CrossRef]
16. Blideran, M.M.; Bertsche, G.; Henschel, W.; Kern, D.P. A mechanically actuated silicon microgripper for handling micro- and nanoparticles. *Microelectron. Eng.* **2006**, *83*, 1382–1385. [CrossRef]
17. ANSYS Inc. (s.f.). Parametric Analysis: The Key to Rapid, Robust Design. Obtenido de White Paper. Available online: https://www.ansys.com/-/media/ansys/corporate/resourcelibrary/whitepaper/wp-parametric-analysis.pdf?la=en&hash=4445A7D983C59F29A4E470B6D7721C2245948FF0 (accessed on 1 December 2020).
18. Park, D.S.-W.; Nallani, A.K.; Cha, D.; Lee, G.-S.; Kim, M.J.; Skidmore, G.; Lee, J.-B.; Lee, J.-S. A sub-micron metallic electrothermal gripper. *Microsyst. Technol.* **2009**, *16*, 367–373. [CrossRef]

19. Feng, Y.-Y.; Chen, S.-J.; Hsieh, P.-H. Fabrication of an electro-thermal micro gripper using silver-nickel ink. In Proceedings of the 2016 IEEE 29th International Conference on Micro Electro Mechanical Systems (MEMS), Shanghai, China, 24–28 January 2016; Institute of Electrical and Electronics Engineers (IEEE): Piscataway, NJ, USA, 2016; pp. 1141–1144.
20. Shivhare, P.; Uma, G.; Mangalanathan, U. Design enhancement of a chevron electrothermally actuated microgripper for improved gripping performance. *Microsyst. Technol.* **2015**, *22*, 2623–2631. [CrossRef]
21. Voicu, R.-C. An SU-8 Microgripper Based on the Cascaded V-Shaped Electrothermal Actuators: Design, Fabrication, Simulation and Experimental Investigations. In *the Actuators*; Constantin, V., Ed.; IntechOpen: London, UK, 2018; Chapter 2; pp. 25–38.
22. Zhang, R.; Chu, J.; Wang, H.; Chen, Z. A multipurpose electrothermal microgripper for biological micro-manipulation. *Microsyst. Technol.* **2012**, *19*, 89–97. [CrossRef]
23. Ghatkesar, M.K.; Barwich, V.; Braun, T.; Ramseyer, J.-P.; Gerber, C.; Hegner, M.; Lang, H.P.; Drechsler, U.; Despont, M. Higher modes of vibration increase mass sensitivity in nanomechanical microcantilevers. *Nanotechnology* **2007**, *18*, 445502. [CrossRef]
24. Reddy, V.M.; Kumar, G. Design and Analysis of Microcantilevers with Various Shapes Using COMSOL Multiphysics Software. *Int. J. Emerg. Technol. Adv. Eng.* **2013**, *3*, 2250–2459.
25. *Ansys Workbench Multiphysics, version 18*; Isotropic elasticity data; Blacksburg, VA, USA, 2020; Available online: http://www.matweb.com/services/contact.aspx (accessed on 12 December 2020).
26. Caballero, A.A.; Yen, K.K. The Use of Micro-Electro-Mechanical Systems (MEMS) in the Construction Industry. In Proceedings of the 20th ISARC, Eindhoven, Holland; 2003; pp. 161–165, ISBN 978-90-6814-574-8. Available online: http://www.irbnet.de/daten/iconda/CIB13324.pdf (accessed on 1 December 2020).
27. Cecil, J.; Powell, D.; Vasquez, D. Assembly and manipulation of microdevices a state of the art survey. *Robot. Comput. Integr. Manuf.* **2007**, *23*, 580–588. [CrossRef]
28. Yong, Z.; Corigliano, A.; Espinosa, H.D. A Thermal Actuator for Nanoscale In Situ Microscopy Testing: Design and Characterization. *J. Micromech. Microeng.* **2006**, *16*, 242.
29. Kaajakari, V. *Practical MEMS*; Small Gear Publishing: Las Vegas, NV, USA, 2009.
30. Espinosa, H.D.; Zhu, Y.; Moldovan, N. Desing and Operation of a MEMS-Based Material Testing System for Nanomechanical Characterization. *J. Microelectromech. Syst.* **2007**, *16*, 1219–1231. [CrossRef]
31. Dochshanov, A.; Verotti, M.; Belfiore, N.P. A Comprehensive Survey on Microgrippers Design: Operational Strategy. *J. Mech. Des.* **2017**, *139*, 070801. [CrossRef]
32. Nikoobin, A.; Niaki, M.H. Deriving and analyzing the effective parameters in microgrippers performance. *Sci. Iran.* **2012**, *19*, 1554–1563. [CrossRef]
33. Llewellyn-Evans, H.; Griffiths, C.; Fahmy, A. Microgripper design and evaluation for automated μ-wire assembly: A survey. *Microsyst. Technol.* **2020**, *26*, 1745–1768. [CrossRef]
34. Ali, N.; Shakoor, R.I.; Hassan, M.M. Design, modeling and simulation of electrothermally actuated Microgripper with integrated capacitive contact sensor. In Proceedings of the 2011 IEEE 14th International Multitopic Conference, Karachi, Pakistan, 22–24 December 2011; pp. 201–206.
35. Thangavel, A.; Rengaswamy, R.; Sukumar, P.K.; Sekar, R. Modelling of Chevron electrothermal actuator and its performance analysis. *Microsyst. Technol.* **2018**, *24*, 1767–1774. [CrossRef]
36. Hoang, K.T.; Nguyen, D.T.; Pham, H.-P. Impact of design parameters on working stability of the electrothermal V-shaped actuator. *Microsyst. Technol.* **2020**, *26*, 1479–1487. [CrossRef]
37. Howell, L.L.; Magleby, S.P.; Olsen, B.M.; Wiley, J. (Eds.) *Handbook of Compliant Mechanisms*; John Wiley & Sons: Hoboken, NJ, USA, 2013.
38. Dado, M.; Al-Sadder, S. The elastic spring behavior of a rhombus frame constructed from non-prismatic beams under large deflection. *Int. J. Mech. Sci.* **2006**, *48*, 958–968. [CrossRef]
39. Voicu, R.; Müller, R.; Eftime, L. Design optimization for an electro-thermally actuated polymeric microgripper. In Proceedings of the 2008 Symposium on Design, Test, Integration and Packaging of MEMS/MOEMS, Cannes, France, 9–11 April 2008; EDA Publishing/DTIP 2008. pp. 182–186.
40. Modeling Natural and Forced Convection in COMSOL Multiphysics®. Available online: https://www.comsol.com/blogs/modeling-natural-and-forced-convection-in-comsol-multiphysics/ (accessed on 4 March 2019).
41. Coutinho, I.T.; Neves, A.A.R.; Sombrio, G.; Souza, J. Surface tension driven flow forming aluminum oxide microtubes. *Int. J. Heat Mass Transf.* **2018**, *126*, 32–38. [CrossRef]

42. Sankar, A.R.; Jency, J.G.; Das, S. Design, fabrication and testing of a high performance silicon piezoresistive Z-axis accelerometer with proof mass-edge-aligned-flexures. *Microsyst. Technol.* **2011**, *18*, 9–23. [CrossRef]
43. Aravind, T.; Ramesh, R.; Ramya, S.; Praveenkumar, S.; Kalaiarasi, A. Comparison of Different Materials on Performance of Chevron Shaped Electrothermal Microgripper. *Int. J. Print. A Packag. Allied Sci.* **2016**, *4*, 2560–2566.
44. Anis, Y.H.; Cleghorn, W.L.; Mills, J.K. Modal Analysis of Microgrippers used in Assembly of MEMS Devices. In Proceedings of the 2005 International Conference on MEMS, NANO and Smart Systems (ICMENS'05), Banff, AB, Canada, 24–27 July 2005.

Publisher's Note: MDPI stays neutral with regard to jurisdictional claims in published maps and institutional affiliations.

© 2020 by the authors. Licensee MDPI, Basel, Switzerland. This article is an open access article distributed under the terms and conditions of the Creative Commons Attribution (CC BY) license (http://creativecommons.org/licenses/by/4.0/).